Statics and Aerodynamics of Lifting Decelerators

L. H. TOWNEND*
Royal Aircraft Establishment, Farnborough, Hants, England

At super and hypersonic speeds, lifting decelerators may take the form of parawings or two-dimensional "sails." For freestream Mach numbers between 10 and 4, an analysis is made of the profiles assumed and isentropic waves produced in nonviscous flows by two-dimensional sails, under pure tension and of finite weight. At the higher freestream Mach numbers, large parts of the compression flow are virtually centered, and even for long sails (e.g., 100 ft chord) at a high Mach number (e.g., 10) and low stress (e.g., 5 tons/in.^{2}), the weight of such a membrane need not exceed 1 lb/ft^2. The two-dimensional analysis can include the effects of skin friction, and is extended to singly-curved "caret" sails, which allow leading edges to be swept but can still produce two-dimensional waves; equilibrium can still be maintained by appropriately applied tensile forces. Experimental evidence on two-dimensional, rectangular sails tends to support the theoretical predictions that much of the sail compression flow will be nearly centered.

Nomenclature

c_f	=	skin-friction coefficient
k	=	$[(\gamma - 1)/(\gamma + 1)]^{1/2}$
M	=	local Mach number
M_n	=	component of freestream Mach number normal to shock wave
p	=	static pressure
p_T	=	stagnation pressure
P	=	elemental pressure forces (Fig. 10)
q	=	kinetic pressure
r	=	radius vector in Prandtl-Meyer wave
s	=	sail arc length
T,T_1,T_2	=	sail tensions
w	=	sail weight per unit material area
x,y	=	see Fig. 3a
x',y',z'	=	see Figs. 9 and 10
y_1',y_2'	=	see Fig. 10d
Λ	=	true sweep of wedge-spar leading edge
β	=	$(M^2 - 1)^{1/2}$
γ	=	ratio of specific heats
ζ	=	shock wave angle $[\sin^{-1}(M_N/M_\infty)]$
η_{KE}	=	kinetic energy efficiency
θ,θ_c,Θ	=	see Fig. 3
μ	=	Mach angle $[\sin^{-1}(1/M)]$
ν	=	Prandtl-Meyer streamline angle
τ	=	see Fig. 10
ϕ	=	Prandtl-Meyer ray angle (see Fig. 1d)

Subscripts

l	=	lower surface of sail
comp	=	sail flow discharge conditions
o	=	sonic conditions
u	=	upper surface of sail
1	=	conditions beneath wedge-spar
∞	=	conditions in freestream

I. Introduction

ALTHOUGH the trajectory of a high-speed load can be greatly modified by the drag of an aerodynamic decelerator, further control could be achieved by the provision of lift or side forces. In particular, the load could be steered, and/or allowed to glide. Thus, in practice, "lifting decelerators" are of considerable interest (see, for example, American work on the supersonic parawing[1–9]), and have been studied in theoretical work, both in parawing form and as two-dimensional "sails" ([see Hayes and Probstein[10] and Figs. 1a and 1b)].

In 1958, Daskin and Feldman[11] examined the aerodynamic properties and geometric form of a rectangular sail, which they assumed to produce a two-dimensional influence on a hypersonic flow. Their analysis was based on a modified Newtonian approximation[12] and they assumed that the sail was of negligible weight and stiffness, that tension was constant (i.e., that skin friction was also negligible) and that sail porosity and boundary-layer growth (or separation) were negligible. In 1959, Fink[13] produced a linearized analysis of the impermeable sail in supersonic flow; in 1960, Boyd[14] extended the analysis of Daskin and Feldman by including Busemann's centrifugal correction to Newtonian flow and in a second paper,[15] re-analyzed the supersonic sail by means of simple wave theory according to Busemann's second-order approximation. In 1961 Boyd[16] analyzed the hypersonic parachute, and in 1962 and 1963, investigated[17,18] the effects of porosity. In 1967, Heynatz and Zierep[19] analyzed the two-dimensional nonporous sail, at small angles of attack and small slopes only, but at freestream Mach numbers in the range from transonic to hypersonic, and included a study of sail stability. Also in 1967, the present author analyzed[20] the two-dimensional sail, not by the use of hypersonic approximations but on the basis of shock and isentropic compression theory, and extended the study to certain three-dimensional sails; the present paper summarizes that analysis and presents 1) typical examples of the profiles assumed, waves produced and forces sustained by sails of various weights, 2) estimates of membrane weight for various flight conditions, and 3) a schlieren photograph of a supersonic sail flow produced in shock-tunnel tests by Cox.[21]

II. Rectangular Sails

A sample sail shape (calculated as by Boyd,[14] using a Newton-Busemann pressure law) is shown in Fig. 1d; this exhibits a rapidly increasing curvature, which is typical of sails at high Mach number and constant tension. For Newtonian flow, the shock must of course coincide with the sail profile—however, if the sail shape and its real flow (a plane

Presented as Paper 68–945 at the AIAA Deceleration Systems Conference, El Centro, Calif., September 23–25, 1968; submitted March 14, 1969; revision received October 9, 1969. The author wishes to thank E. G. Broadbent and C. C. L. Sells for valuable comments on membrane statics, and M. G. Joyce for program writing and production of all data presented in this paper.

* Senior Scientific Officer, Aerodynamics Department.

shock on the wedge spar and an isentropic sail compression) were accurately calculated, one might expect (from, for example, Boyd's results) that the isentropic wave might quite closely resemble a reversed Prandtl-Meyer wave, and so might produce "nearly centered" compression. This possibility is examined first.

For a sail of constant tension and zero weight to produce precisely centered compression, 1) its shape must be that of a Prandtl-Meyer streamline[20] ($r/r_o = \sec^{1/k^2} k\phi$ in Figure 1d), and 2) from geometry and the membrane equation (i.e., static pressure difference = $Td\theta/ds$) the required distribution of static pressure difference is[20]

$$\frac{(p_l - p_u)}{T} = \left(\frac{1}{k^2} - 1\right) \frac{\tan^2 k\phi \cos^{1/k^2} k\phi}{[1 + (1/k^2)\tan^2 k\phi]^{3/2}}$$

Since the lower surface static pressure will be

$$\frac{p_l}{p_T} = \left(1 + \frac{\gamma - 1}{2} M^2\right)^{-\gamma/(\gamma-1)} = \left(1 - \frac{k^2}{k^2 - 1}\left[1 + \frac{1}{k^2}\tan^2 k\phi\right]\right)^{-(k^2+1)/2k^2}$$

the upper surface static pressure must be

$$\frac{p_u}{p_T} = \left(1 - \frac{k^2}{k^2 - 1}\left[1 + \frac{1}{k^2}\tan^2 k\phi\right]\right)^{-(k^2+1)/2k^2} - \left(\frac{1}{k^2} - 1\right) \frac{\tan^2 k\phi \cos^{1/k^2} k\phi}{[1 + (1/k^2)\tan^2 k\phi]^{3/2}} \frac{T}{p_T r_0}$$

Airflow function — Membrane function

Thus, in Fig. 2 the vertical distance by which a point on the curve for the airflow function lies above a particular membrane curve, corresponds to the local value required of p_u/p_T. By appropriate selection of $p_T r_o/T$, a membrane curve can be aligned quite closely with the airflow curve, at least over a limited Mach number range—this means that, in this range, p_u/p_T need not vary much to maintain centered compression, or perhaps, that a sail with zero or constant pressure on the upper surface should produce a nearly centered wave on the lower. From Fig. 2, it seems that this will not occur at low Mach numbers ($k\phi < 25°$, $M < 1.5$ approximately). However, it seems likely to occur at the higher Mach numbers at which lifting decelerators might be deployed†—whether it occurs to a significant extent on practical sails having realistic upper surface pressures and finite weight can be studied as part of the more general question of what types of wave and what contributions to lift and drag such sails can provide.

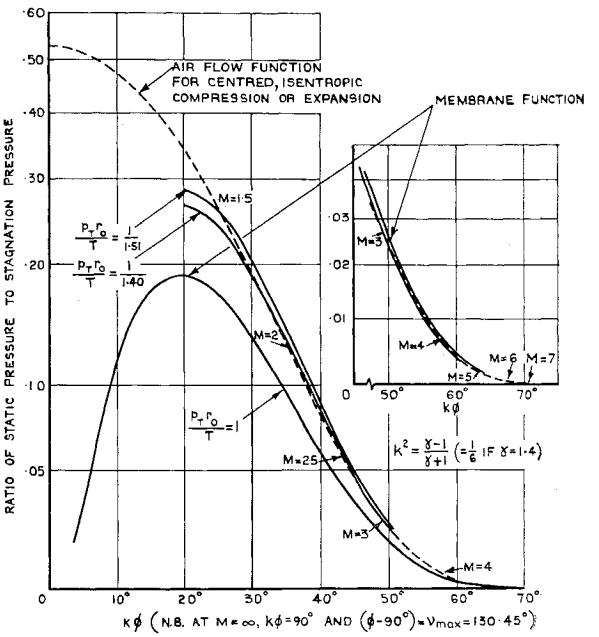

Fig. 2 Variation with local Mach number of aerodynamic and geometric properties for a sail producing centered compression.

A. General Case

Consider the equilibrium of an element of a two-dimensional sail (see Fig. 3a) which is of negligible stiffness and subject to negligible increments in static pressure caused by porosity, or boundary layer thickness or separation. Then the forces in Fig. 3b must be in equilibrium as follows:

$$T\cos(d\theta/2) = (T + dT)\cos(d\theta/2) + wds\sin(\theta + \theta_c) + q_\infty c_f ds$$

$$(p_l - p_u)ds = (2T + dT)\sin(d\theta/2) + wds\cos(\theta + \theta_c)$$

note that skin friction has been assumed to act on one side of the sail only, since the low pressure side will probably be washed by recirculating flows of low velocity. At high supersonic and hypersonic speeds, skin friction is likely to be significant; on the other hand, the contribution of sail weight to sail tension [aforementioned $wds\sin(\theta + \theta_c)$] should be negligible compared with tensions already induced by flow compression. Thus, the equations become

$$dT/ds = -q_\infty c_f,\ Td\theta/ds = p_l - [p_u + w\cos(\theta + \theta_c)],$$

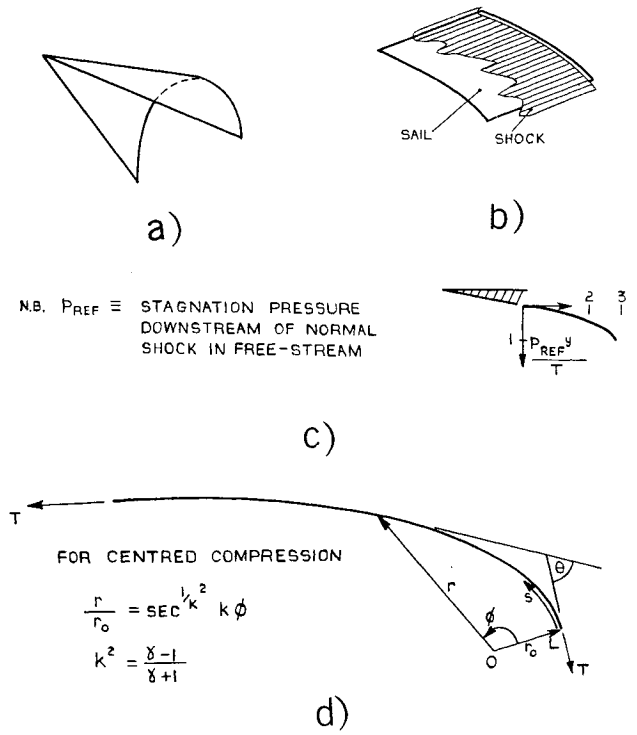

Fig. 1a) NASA parawing (straight leading edges); b) two-dimensional sail in Newtonian flow; c) typical sail profile (Boyd[14]); and d) sail producing centered compression.

† In an alternative analysis, Pike[22] has compared the radius of curvature of a Prandtl-Meyer streamline with that of a sail having constant tension, zero weight, and zero upper surface pressure; Pike shows that, for $\gamma = 1.4$ and $M > 7$, these radii differ by less than 3%, and that as $M_\infty \to \infty$ their difference tends to zero.

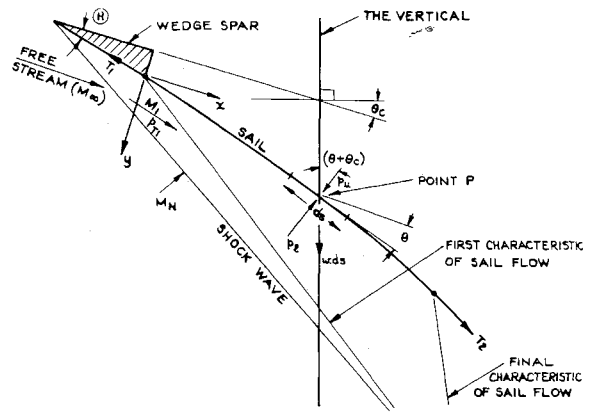

Fig. 3a Sail model analyzed.

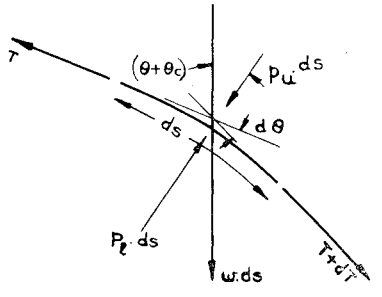

Fig. 3b Sail element of unit width and length, *ds*.

from which elimination of T gives

$$\frac{ds}{d\theta} = \frac{dx}{\cos\theta d\theta} = \frac{dy}{\sin\theta d\theta} = k'' \exp(I), \frac{1}{k''} = \frac{p_{T_1}B}{T_{l.e.}}$$

$$B = \left[\left(1 + \frac{\gamma - 1}{2} M_1^2\right)^{-\gamma/(\gamma-1)} - \frac{p_u + w\cos(\Theta + \theta_c)}{p_{T_1}}\right],$$

$$I \equiv -\int \frac{q_\infty c_f + d/d\theta\{p_l - [p_u + w\cos(\theta + \theta_c)]\}}{\{p_l - [p_u + w\cos(\theta + \theta_c)]\}} d\theta$$

Thus the sail profile is given by

$$\frac{p_{T_1}x}{T_{l.e.}} = \int_{\beta_1}^{\beta} \frac{\exp(I)}{B} \cos\theta \left(\frac{1}{1+\beta^2} - \frac{1}{1+k^2\beta^2}\right) d\beta$$

$$\frac{p_{T_1}y}{T_{l.e.}} = \int_{\beta_1}^{\beta} \frac{\exp(I)}{B} \sin\theta \left(\frac{1}{1+\beta^2} - \frac{1}{1+k^2\beta^2}\right) d\beta$$

in which $\theta = \Theta + (1/k)\tan^{-1}k\beta_1 - \tan^{-1}\beta_1 - (1/k)\tan^{-1}k\beta + \tan^{-1}\beta$.

If skin friction is negligible, then

$$\frac{\exp(I)}{B} = \left\{\left[1 + \frac{\gamma - 1}{2}(1 + \beta^2)\right]^{-\gamma/(\gamma-1)} - \frac{p_u + w\cos(\theta + \theta_c)}{p_{T_1}}\right\}^{-1}$$

and the aforementioned integrals are modified accordingly. For this condition, which gives rise to constant tension, typical sail profiles and associated flows are shown in Figs. 4–7.

In Fig. 4a, for $p_u/p_\infty = 0$, $M_N = 1$ (i.e., fully isentropic flow) and $w/p_\infty = 0$, 0.2 and 0.4, sail profiles are drawn for freestream and discharge Mach numbers (M_∞ and M_{comp}) of 10 and 3.5, respectively; sail profiles are shown in the top two sketches, firstly in terms of $p_{T_1}x/T$ and $p_{T_1}y/T$, and secondly, for direct comparison at equal chord. Sketch A confirms that curvature increases rapidly towards the trailing edge and also that, as sail weight rises, then, for a given extent of compression $p_{T_1}x/T$ also rises, so that, for given values of p_{T_1} and sail chord, tension is consequently reduced. Sketch B shows that, the heavier the sail, the more rapid is the rate of increase of curvature towards the trailing edge, with the result that, since regions of small dy/dx extend over larger proportions of the chord, the heavier but more moderately tensioned sails lie above the lighter sails. From this fact it also follows that for the heavier sails, the first characteristic of the sail flow (i.e., that at which streamline curvature is initiated) lies further from the trailing edge; but in the three drawings showing wave positions (for $p_u/p_\infty = 0$ and $w/p_\infty = 0$, 0.2 and 0.4, and for sail chords of approximately 100 in.), it is further seen that compression waves corresponding to local Mach numbers between 7 and 3.5 are nearly centered.‡ In Fig. 4b, the effect of changing the upper surface pressure to $p_u/p_\infty = 0.5$, is seen to be a significant change in the positions of initial waves, but little change in the centering of later waves. Finally Fig. 4c shows, for two values of p_u/p_∞, the lifting effectiveness (C_L) and efficiency (L/D) of sails in nonviscous flow at $M_\infty = 10$, and also at $M_\infty = 7$ and 4. The wedge-spar is assumed to be extremely thin, so that the forces and flow losses it produces may be neglected; the lift coefficient may then be written as

$$C_L = T\sin(\nu_\infty - \nu_{comp})/(q_\infty x) = \sin(\nu_\infty - \nu_{comp})/[(q_\infty/p_{T_\infty})(p_{T_\infty}/p_{T_1})(p_{T_1}x/T)]$$

in which $(\nu_\infty - \nu_{comp})$ is the angle through which the sail turns the flow; lift-to-drag ratio in nonviscous flow is $(L/D)_{const\ T} = \sin(\nu_\infty - \nu_{comp})/[1 - \cos(\nu_\infty - \nu_{comp})]$ or $\cot[(\nu_\infty - \nu_{comp})/2]$, and with axis variables C_L and L/D, lines of constant drag coefficient are easily constructed. Because of the assumptions in this example that the flow is isentropic throughout (i.e., $p_{T_1} = p_{T_\infty}$), local values of static

Table 1 Values of sail and flow parameters

M_∞, M_{comp}	M_N, η_{KE}, Θ and M_1	p_u/p_∞	w/p_∞	$p_{T_1}x/T$	Fig. No.
10	$M_N = 1$ $\eta_{KE} = 1$ $\Theta = 0°$ $M_1 = 10$	0	0	3500	4a
			0.2	3875	
			0.4	4393	
		0.5	0	4743	4b
			0.2	5799	
			0.4	8410	
3.5	$M_N = 1.4$ $\eta_{KE} = 0.999$ $\Theta = 3.264°$ $M_1 = 8.870$	0.5	0	1991	5
			0.2	2110	
			0.4	2252	
		1.0	0	2336	
			0.2	2533	
			0.4	2789	
7	$M_N = 2.0$ $\eta_{KE} = 0.990$ $\Theta = 10.22°$ $M_1 = 5.196$	0.5	0	91.07	6
			0.2	93.47	
			0.4	96.04	
2.5		1.0	0	97.61	
			0.2	100.5	
			0.4	103.6	
4	$M_N = 1.2$ $\eta_{KE} = 0.999$ $\Theta = 4.265°$ $M_1 = 3.690$	0.5	0	24.31	7
			0.2	26.79	
			0.4	30.16	
1.5		1.0	0	32.56	
			0.2	39.22	
			0.4	54.49	

‡ In practice, convergent characteristics would coalesce into a shock wave, together with a reflected wave which would be either an expansion or a compression, according to the value of M_∞ and the extent of compression caused by the sail. For clarity of Figs. 4–7, interactions are not shown.

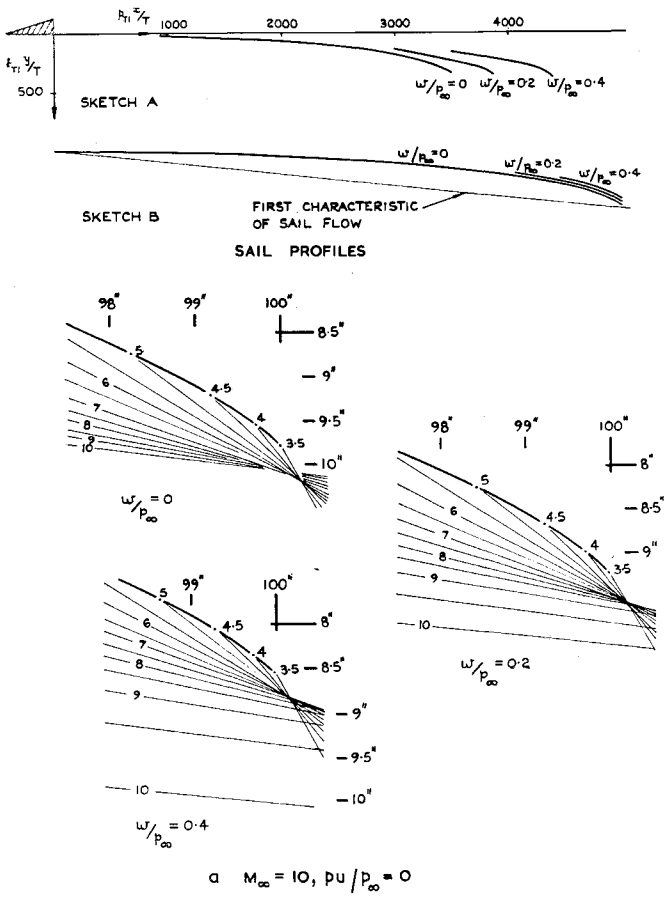

Fig. 4a Two-dimensional, isentropic sail (i.e., $M_N = 1$), as influenced by weight and upper surface pressure.

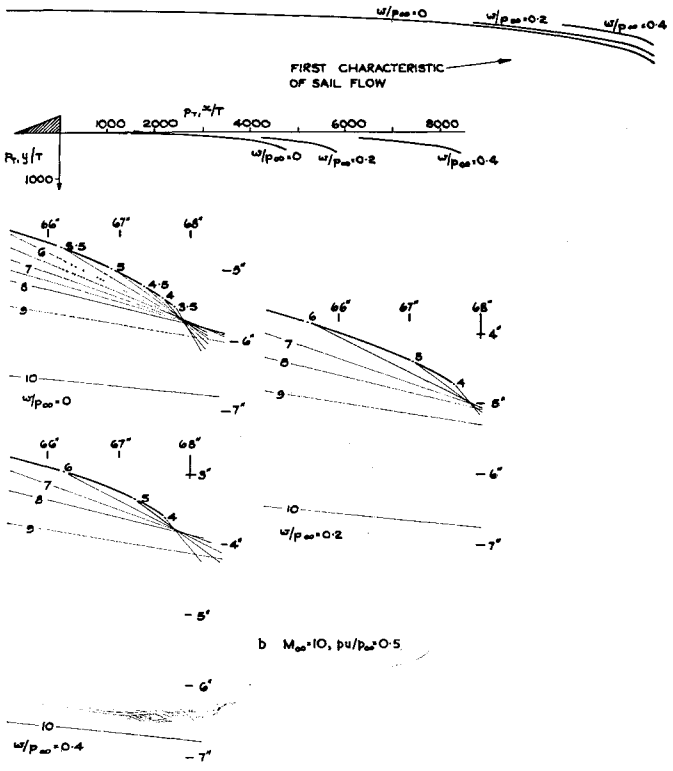

Fig. 4b Two-dimensional, isentropic sail (i.e., $M_N = 1$), as influenced by weight and upper surface pressure.

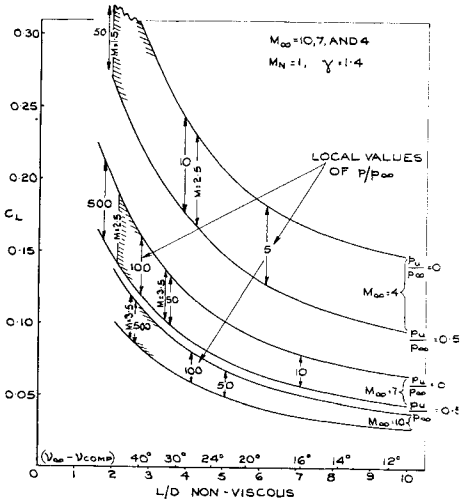

Fig. 4c Two-dimensional, isentropic sail (i.e. $M_N = 1$), as influenced by weight and upper surface pressure.

pressure ratio are given as

$$\frac{p}{p_\infty} = \frac{p}{p_{T_1}}\frac{p_{T_\infty}}{p_\infty} = \left(\frac{2 + (\gamma - 1)M_\infty^2}{2 + (\gamma - 1)M^2}\right)^{\gamma/(\gamma-1)}$$

thus lines of constant static pressure ratio can also be easily constructed on Fig. 4c, and the likelihood of boundary-layer separation assessed.[23]

If at $M_\infty = 10$, a sail is mounted behind a wedge-spar producing a shockwave ($M_N = 1.4$ in Fig. 5), the effects of w/p_∞ on sail profile and its position relative to the first characteristic of the sail flow (see Sketch B) are much reduced, nearly centered compression being obtained over a similar range of local Mach number; with $M_N = 2.6$, the effects of w/p_∞ on profile are extremely small.[20]

As seen from Figs. 4 and 5, $p_{T_1}\, x/T$ always increases with w/p_∞ if other parameters are constant. In Figs. 6 and 7 ($M_\infty = 7$ and 4, respectively) plots of $p_{T_1}\, x/T$ are not shown since this trend is unchanged. The effects of w/p_∞ on sails at $M_\infty = 7$ and low M_N are significant,[20] but even for $w/p_\infty = 0$, initial compression waves lie well below the near-focus of waves in the range $5 \geq M \geq 2.5$. If M_N is increased to 2 (see Fig. 6) the effects of variations in w/p_∞ are slight. Much of the compression flow is nearly centered. For sails operating at $M_\infty = 4$ and $M_N = 1.2$ (see Fig. 7) the influence of w/p_∞ is considerable but, even at $w/p_\infty = 0$ and for the rather short sail drawn, initial waves lie well below the points at which later waves intersect, and no part of the compression flow can be described as centered; if $M_N = 1.6$, the influence of w/p_∞ is reduced[20] but again, even for weightless sails, initial waves lie below the intersections of later waves, and even the latter are not closely centered.

It is tentatively concluded from Figs. 4–7 and from others[20] that: 1) in nonviscous hypersonic flows, significant extents of nearly centered compression may exist beneath sails in pure tension; 2) as freestream Mach number falls to supersonic values, centering of the waves becomes less marked; 3) at a given freestream Mach number, increases in upper surface pressure and/or sail weight usually increase the gaps between initial compression waves and the near-focus of later waves; and 4) at a given freestream Mach number, an increase in the wedge-spar angle reduces the influence of upper surface pressure and of sail weight.

It has been shown that a combination of M_∞, M_N, w/p_∞ and p_u/p_∞ leads as a mathematical requirement to a particular value (see Table 1) of $p_{T_1}\, x/T$; the engineering acceptability of these combinations is now examined.

For a sail tethered to the trailing edge of a wedge-spar

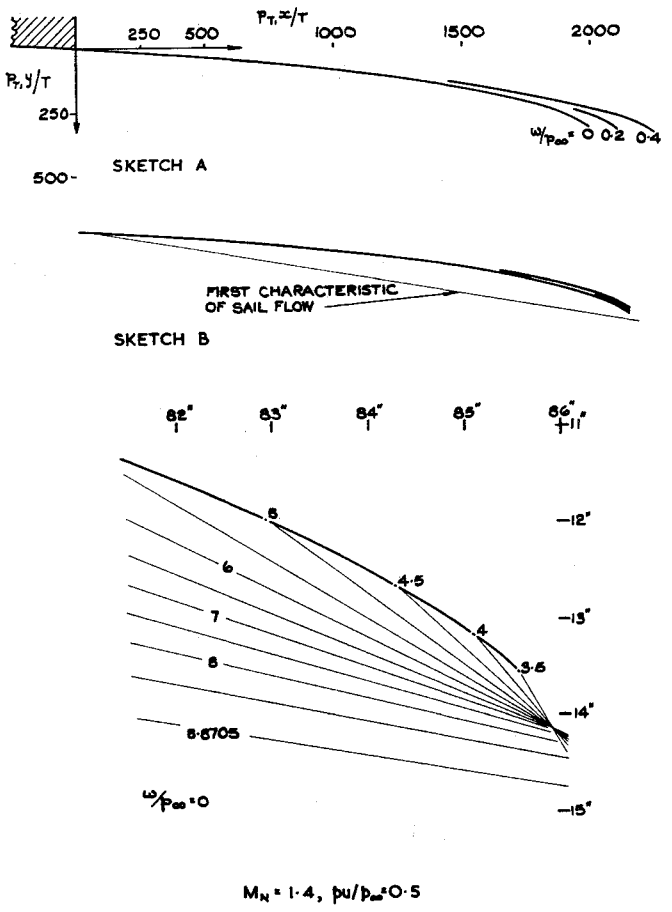

Fig. 5 Two-dimensional, wedge-spar-plus-sail at $M_\infty = 10$.

as in Fig. 3, one may write[20]

$$\frac{p_{T_1}x}{T} \equiv \left[\frac{2 + (\gamma - 1)M_\infty^2}{2 + (1 - \eta_{KE})(\gamma - 1)M_\infty^2}\right]^{\gamma/(\gamma-1)} \frac{p_\infty x}{T}$$

in which, for a given value of M_∞, 1) η_{KE} prescribes the strength of the shock on the wedge-spar and, hence, M_N and M_1, 2) p_∞ implies an equivalent air speed (EAS), and 3) x is the sail chord. If these parameters are allotted numerical values, then for a chosen $p_{T_1}x/T$, a particular value will result for T, the sail tension per foot span. For example, in Fig. 8 the variation with T of $p_{T_1}x/T$ is shown for sails having $x = 1$, 10 and 100 ft, and operating at $M_\infty = 10$, 7 and 4 and identical values of EAS (350 knots); the effects of varying shock strength are indicated by η_{KE} values of 1.0 and 0.99 (see Table 1). Extra scales indicate 1) the thickness of sails which would operate at specified tensile stresses (5 tons/in.^{2} and 10 tons/in.^{2}), and 2) the sail weight per unit wetted area which would result for a sail material such as high quality stainless steel (which has a density of 0.28 lb/in.^{3}). Note that, even for the lower stress level (5 tons/in.^{2}), sail thickness and weight need not exceed values of 0.05 in. (approximately 18 swg) and 2 lb/ft^2, respectively; the corresponding value of sail tension or spar loading is about 7000 lb/ft span.

Values of $p_{T_1}x/T$ for realistic operating conditions lie between 10 and 10000; thus the values of $p_{T_1}x/T$ required in Figs. 4–7 (lying in the "boxes" on Fig. 8 and listed in Table 1) can be compatible with engineering realism. For 350 knots EAS, $w/p_\infty = 0.4$ would frequently be too high a sail weight, even for stress levels as low as 5 tons/in.^{2} In Ref. 20, tabulated values of EAS and p_∞ show how, at various values of M_∞, the flight environment would vary—with these values of p_∞ in the foregoing equation, Fig. 8 could be redrawn for EAS $\neq$ 350 knots.

III. Caret Sails

At design conditions of Mach number and incidence, two-dimensional, centered, isentropic waves can in principle[24] be formed by and contained between so-called "caret" surfaces; if the leading edges of such surfaces are straight, each surface is conically curved through the tip. Surfaces of single but nonconical curvature may also produce and contain two-dimensional but noncentered isentropic waves (see Fig. 9a). Both types may be individually wrapped from initially flat flexible foils of correct developed planform. Suitably tethered, such a foil can form a caret sail, though any element (such as E in Fig. 9b) will require not only chordwise tensions, but transverse tensions to counter the side force caused by anhedral.

Consider the geometry of element E. The axis $0y'$ is the focal line of the compression waves from AD and BC (i.e., the "instantaneous focal line" for a part of a noncentered flow); $0x'$ and $0z'$ form an orthogonal system of axes with $0y'$, in which system $0x'$ is aligned with the inflow direction (given by M_1 or $k\phi_1$), so that $0z'$ is then at a defined angle to the sonic plane ($M = 1$, $k\phi = 0$) of the given two-dimensional flow. Suppose that the caret sail profile corresponds to streamline S; further, for isentropic compression from M_1 to M by a centered (i.e., reversed Prandtl-Meyer) wave, suppose the streamline through element E is S′, with whose center of compression that of S is instantaneously coincident: finally, let streamline S″ be that with which a two-dimensional sail, producing isentropic compression from M_1 to M, would align itself. Since all three waves correspond to isentropic compression from the same initial value of Mach number, their sonic lines are parallel, but not in general colinear. It is clear that an element of length ds and projected width dy', situated at the point at which S, S′ and S″ are tangential, will for all these streamlines, form projections onto the plane

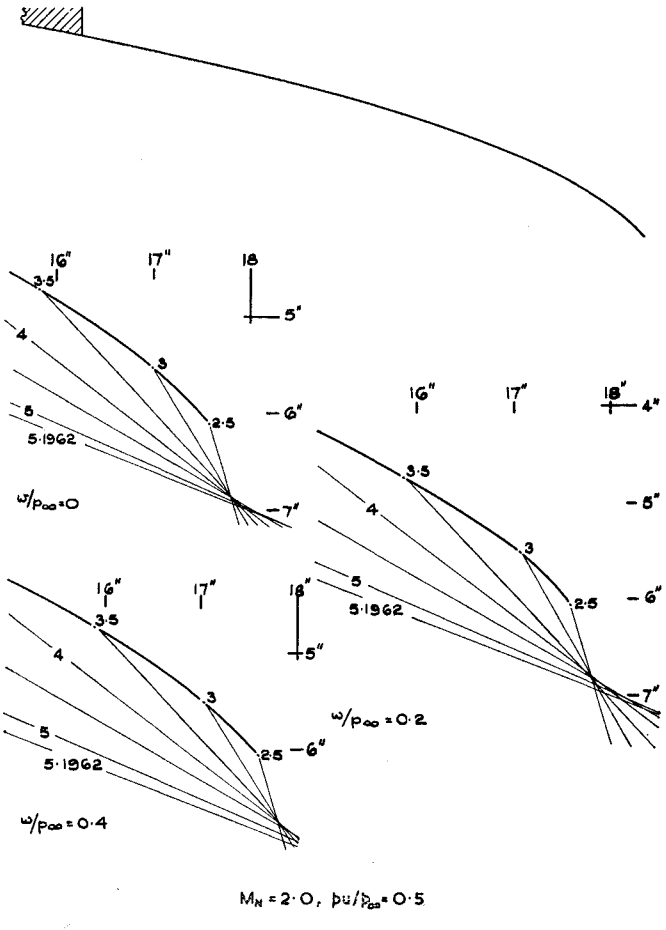

Fig. 6 Two-dimensional, wedge-spar-plus-sail at $M_\infty = 7$.

$x'\ 0y'$, which are of different geometries (rectangular for S′ and S″, and trapezoidal for S) but of equal area: similarly the rectangular and trapezoidal projections onto the plane $z'0y'$ will all be of equal area. Since the pressure on the element is identical for all these streamlines, the components of pressure force parallel to $0x'$ and $0z'$ are identical; it follows that, if any differences arise between the profiles and/or statics of two-dimensional sails and caret sails, these must be caused by the third component of pressure force (or to differences in wetted area).

Of the pressure force on element E, the component P_z' (parallel to $0z'$) and P_x' (parallel to $0x'$), being equal to those on a corresponding element of a two-dimensional sail, will produce a resultant (P_{xz}' in Fig. 10) which is identical in magnitude [$= (p_l - p_u)dsdy$] and direction (parallel to $x'0z'$ and normal to streamline S). The third component P_y' is, by definition, parallel to $0y'$ and so lies in the same plane as $0y'$ and the surface generator which passes, as a straight line, through the point 0 and the centroid of element E. P_y' may thus be replaced by two statically equivalent forces P_r and P_g, of which P_g lies along the generator and is such that P_r lies parallel to $x'0z'$; since P_r passes through the axis $0y'$, the angle between P_r and the streamline S must equal the Mach angle, $\mu = \sin^{-1}(1/M)$. Thus in the plane which contains the streamline S, both P_r and P_{xz}' can be shown (see Fig. 10b). P_r is seen to contribute two components, one which is directly additive to P_{xz}' and is given by $P_r' = P_r \sin\mu = P_r/M$, and one which acts tangentially along the sail chord,

$$P_r'' = P_r \cos\mu = P_r(M^2 - 1)^{1/2}/M = P_r'(M^2 - 1)^{1/2}$$

But from caret geometry [Fig. 10c],

$$P_r/P_{xz}' = \cot^2\tau \sin\mu = K[1 + k^2(M^2 - 1)]^{1/k^2}/M$$

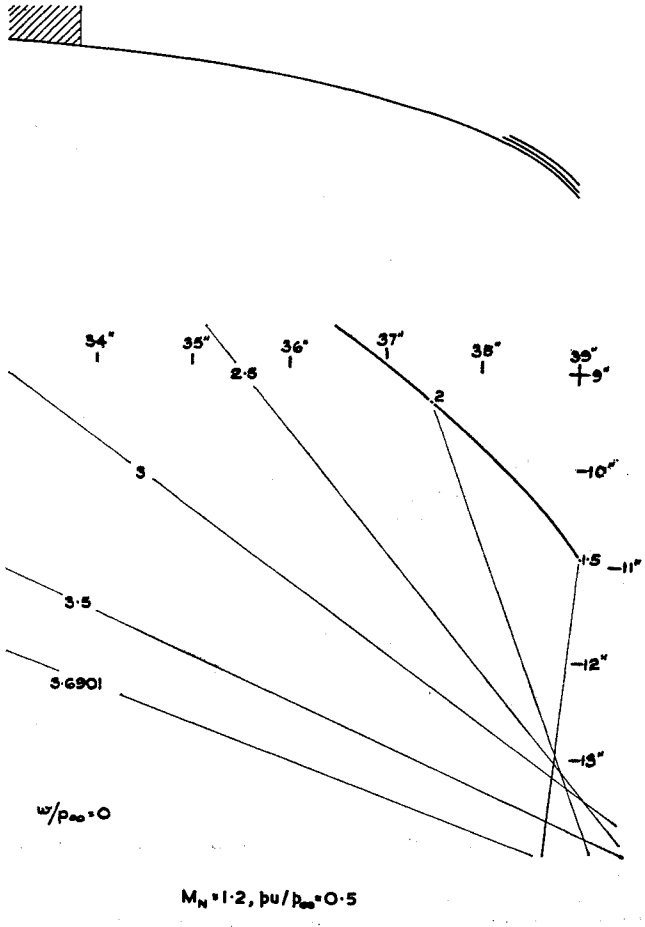

Fig. 7 Two-dimensional, wedge-spar-plus-sail at $M_\infty = 4$.

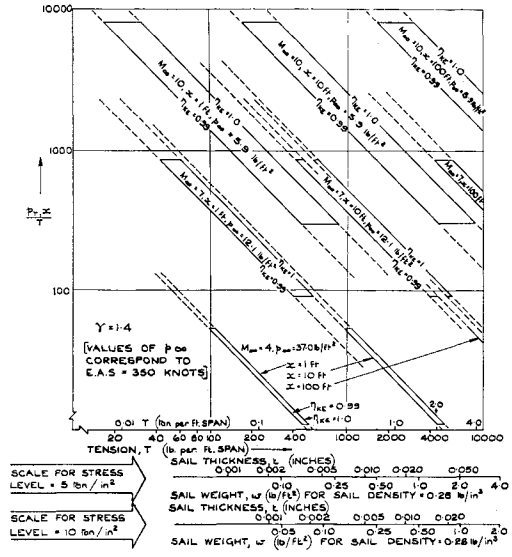

Fig. 8 Sail tension, stress, thickness and weight.

and

$$K = \left[\frac{2 + (\gamma - 1)M_N^2}{2\gamma M_N^2 - (\gamma - 1)}\right] \frac{\sin^2\Lambda}{\cos^2\zeta - \sin^2\Lambda} \times \frac{1}{[1 + k^2(M_1^2 - 1)]^{1/k^2}}$$

(= 0 for rectangular sails)

Thus

$$P_r'P_{xz}' = (1/M)P_r/P_{xz}' = K[1 + k^2(M^2 - 1)]^{1/k^2}/M^2$$

and

$$P_r''/P_{xz}' = (M^2 - 1)^{1/2}P_r'/P_{xz}'$$

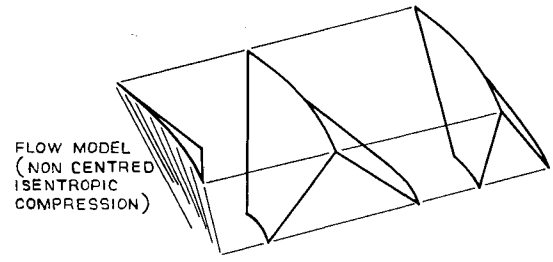

Fig. 9a Nonconical, singly curved caret surfaces.

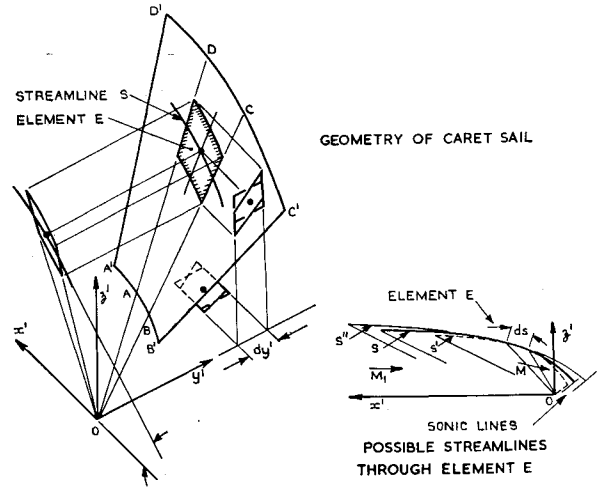

Fig. 9b Aerodynamic and geometric features of a caret sail.

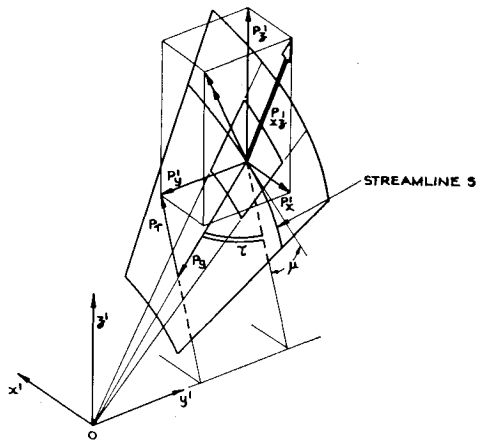

Fig. 10a Components of the pressure force on element E.

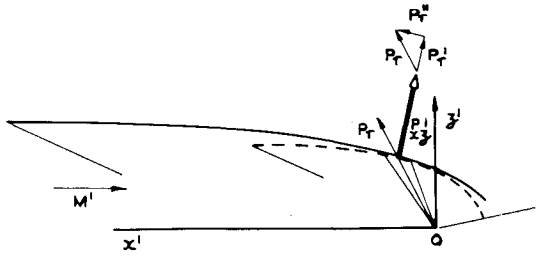

Fig. 10b Components parallel to the plane $x'Oz'$.

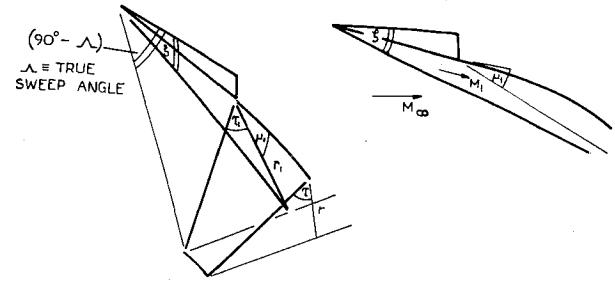

Fig. 10c Geometry of wedge-spar-plus-sail.

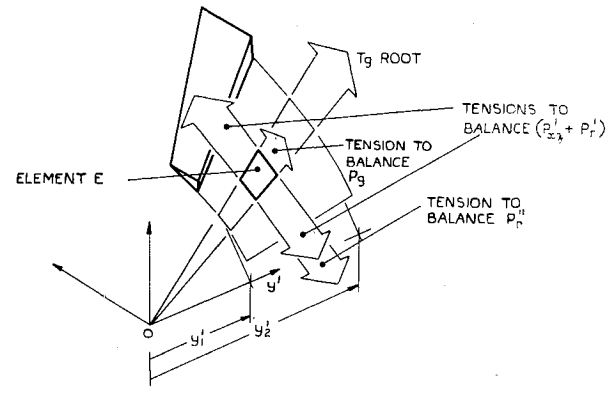

Fig. 10d Tensions to balance pressure force on element E

The forces P_r, P_r', P_r'', and P_{xz}' can now be related[20] to sail tension, skin friction and the weight of element E. If $w \sin(\theta + \theta_c)$ is again neglected together with skin-friction drag since boundary-layer cross-flows[24] cannot as yet be calculated except for laminar flow on conically curved carets,[25,26] analysis (which is two-dimensional[20]) gives the sail profile as

$$\frac{p_{T_1}x}{T_{l.e.}} = \int_\Theta^\theta \frac{p_{T_1}}{E} \exp\left\{\int_\Theta^{\bar\theta} \frac{(p_l - p_u)}{E} \times \frac{K}{M^2}(M^2-1)^{1/2}[1 + k^2(M^2-1)]^{1/k^2} d\bar\theta\right\} \cos\bar\theta d\bar\theta$$

$$\frac{p_{T_1}y}{T_{l.e.}} = \int_\Theta^\theta \frac{p_{T_1}}{E} \exp\left\{\int_\Theta^{\bar\theta} \frac{(p_l - p_u)}{E} \times \frac{K}{M^2}(M^2-1)^{1/2}[1 + k^2(M^2-1)]^{1/k^2} d\bar\theta\right\} \sin\bar\theta d\bar\theta$$

in which $T_{l.e.}$ is the tension at the leading edge of the particular spanwise section considered, and

$$E = (p_l - p_u)\{1 + (K/M^2)[1 + k^2(M^2-1)]^{1/k^2}\} - w\cos(\theta + \theta_c)\{1 + (K/M^2)[1 + k^2(M^2-1)]^{1/k^2}\}^{1/2}$$

The remaining force is P_g, which applies tension along the generator; for a given generator, these tensions may be summed to give[20]

$$T_g]_{\text{root}} = (K/M)[1 + k^2(M^2-1)]^{1/k^2} \times (p_l - p_u)(y_2' - y_1')\sec\tau$$

Thus, as shown in Fig. 10d, the components of pressure force on an element of caret sail are such that; 1) some can be resolved along surface generators and so be balanced by tensions at the root, and 2) the remainder lie in a single plane and can be analyzed in two dimensions.

IV. Experimental Results

A two-dimensional model (see Fig. 11a) has been tested by Cox[21] in a hypersonic stream of nitrogen produced in the R.A.E. Shock Tunnel (see Fig. 11a). The model consists of a rectangular wedge at 10° incidence and a rectangular sail of 0.002 in. shim steel; the wedge and the sail are each about 4 in. long. Sails survived the starting loads and the steady running condition, but were torn from the trailing edge support during flow breakdown.

In one test (see Fig. 11b), $M_1 \approx 5$, $R_e \approx 5 \times 10^5$/ft, $M_\infty \approx 7$, and $\Theta \approx 10°$, the flow was turned by the sail through about 30°, and the compression wave seemed to be approximately centered; the static pressure ratio (p_{comp}/p_1) would be about 20 for $\gamma = 1.4$ = constant, provided there was no boundary-layer separation. There is in fact no evidence of separation and, for nitrogen, γ-variation caused by compression would be very slight; thus, the model and test conditions correspond closely to those assumed for Fig. 6 with which Cox's schlieren photograph should be compared. Close examination of the photograph suggests that the rearmost parts of the compression were centered, and that the shock from their focal point intercepted the initial sail flow characteristic, as it happened, near the shock from the wedge-spar. There is, thus, some experimental evidence to support the predictions in this paper that 1) hypersonic sails may produce significant extents of nearly centered compression, and 2) a gap will often exist between initial compression characteristics and the near-focus of those further downstream.

V. Conclusions

For freestream Mach numbers of 10, 7, and 4, rectangular sails in pure tension and of finite weight are predicted to produce two-dimensional isentropic compression waves; for the higher freestream Mach numbers, the downstream parts of these waves are nearly centered. At a given freestream Mach number, an increase in upper surface pressure or sail weight usually increases the gaps between initial compression waves and the near-focus of later waves; if a wedge-spar is attached to the leading edge of a sail, an increase in wedge angle appears to reduce the influence of upper surface pressure and sail weight on sail profile and wave form. In-

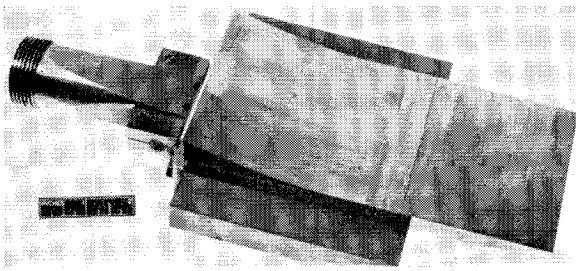

Fig. 11a Sail model (Cox[21]).

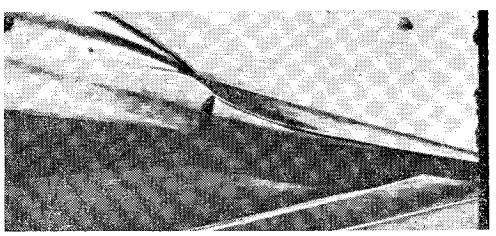

Fig. 11b Schlieren photograph for $M_\infty \cong 7$ (Cox[21]).

vestigation of the structural aspects of two-dimensional sails suggests that, even for long sails (e.g. 100 ft chord) at high Mach number (e.g., 10) and low stress (e.g., 5 tons/in.^{2}), the weight of the membrane need not exceed 1 lb/ft^2.

For caret sails, equilibrium still requires only tensile forces, some directed along the chord of the sail, and some acting at the root and directed along the generators of the singly curved surface.

Experiments at R.A.E. have provided some evidence to support the predictions in this paper that 1) hypersonic sails may produce significant extents of nearly centered compression, and 2) a gap will often exist between initial compression characteristics and the near-focus of those further downstream.

References

[1] Rogallo, F. M. and Lowry, J. G., "Flexible Re-Entry Gliders," Preprint No. 175C, 1960, Society of Automotive Engineers.

[2] Rogallo, F. M., Lowry, J. G., and Croom, D. R., "Preliminary Investigation of a Paraglider," TN D–443, 1960, NASA.

[3] Taylor, R. T., "Wind-Tunnel Investigation of Paraglider Models at Supersonic Speeds," TN D–985, 1961, NASA.

[4] Fournier, P. G. and Bell, B. A., "Transonic Pressure Distributions on Three Rigid Wings Simulating Paragliders with Varied Canopy Curvature and Leading-Edge Sweep," TN D–1009, 1962, NASA.

[5] Penland, J. A., "A Study of the Aerodynamic Characteristics of a Fixed Geometry Paraglider Configuration and Three Canopies with Simulated Variable Canopy Inflation at a Mach Number of 6.6," TN D–1022, 1962, NASA.

[6] Fournier, P. G., "Pressure Distributions on Three Rigid Wings Simulating Parawings with Varied Canopy Curvature and Leading-Edge Sweep at Mach Numbers from 2.29 to 4.65," TN D–1618, 1963, NASA.

[7] Wornom, D. E., "Aerodynamic Characteristics of a Flexible-Canopy Paraglider Model at a Mach Number of 4.5 for Angles of Attack to 360° and Sideslip Angles from 0° to 90°," TN D–1776, 1963, NASA.

[8] Briggs, C., "An Annotated Bibliography on Paragliders," Library Literature Search No. 24, 1963, Martin Company, Denver; also Astia Document 295,143.

[9] Fralich, R. W., "Stress and Shape Analysis of a Paraglider Wing," Preprint No. 64–WA/AV–4, 1964, American Society of Mechanical Engineers.

[10] Hayes, W. D. and Probstein, R. F., *Hypersonic Flow Theory*, 2nd ed., Vol. 1, Academic Press, New York, 1966, pp. 149–152.

[11] Daskin, W. and Feldman, L., "The Characteristics of Two-Dimensional Sails in Hypersonic Flow," *Journal of the Aeronautical Sciences*, Vol. 25, No. 1, Jan. 1958, pp. 53–55.

[12] Lees, L., "Laminar Heat Transfer over Blunt Nosed Bodies at Hypersonic Flight Speeds," *Jet Propulsion*, Vol. 26, No. 4, April 1956.

[13] Fink, M. R., "Analytical Study of the Aerodynamic Performance and Geometric Shape of Two-Dimensional Sails in Supersonic Flow," Rept. M–1275–1, 1959, United Aircraft Corp.

[14] Boyd, E. A., "Busemann Correction to the Characteristics of the Two-Dimensional Hypersonic Sail," Rept. 140, 1960, Cranfield College of Aeronautics.

[15] Boyd, E. A., "The Characteristics of a Two-Dimensional Supersonic Sail," Rept. 143, 1960, Cranfield College of Aeronautics.

[16] Boyd, E. A., "Aerodynamic Characteristics of a Hypersonic Parachute," Rept. 152, 1961, Cranfield College of Aeronautics.

[17] Boyd, E. A., "Effect of Porosity on the Two-Dimensional Supersonic Sail," *Journal of the Aerospace Sciences*, Vol. 29, No. 2, Feb. 1962, pp. 232–233.

[18] Boyd, E. A., "Shape of the Porous Two-Dimensional Hypersonic Sail," *AIAA Journal*, Vol. 1, No. 5, May 1963, pp. 1177–1178.

[19] Heynatz, J. T. and Zierep, J., "Das schwach angestellte Segel bei Überschall-bei Hyperschall-und bei Schallgeschwindigkeit," *Acta Mechanica*, Vol. 3, No. 3, July 1967; also available as "The Sail at Small Angle of Incidence at Supersonic, Hypersonic and Sonic Speed," Royal Aircraft Establishment Translation No. 1329 by L. Klanfer, 1969.

[20] Townend, L. H., "Rectangular and Caret Sails in Supersonic Flow," TR 67006, 1967, Royal Aircraft Establishment; also available as Reports and Memoranda No. 3624, 1970, Aeronautical Research Council, Great Britain.

[21] Cox, S. G., "Flow Visualisation Experiments at $M_\infty \simeq 7$ on a Simply Supported Two-Dimensional Rectangular Sail in the RAE 15 Inch Shock Tunnel," Royal Aircraft Establishment Technical Report to be published.

[22] Pike, J., "A Note on Two-Dimensional Supersonic Sails," Royal Aircraft Establishment Technical Report to be published.

[23] Needham, D. A. and Stollery, J. L., "Hypersonic Studies of Incipient Separation and Separated Flows," *AGARD Conference Proceedings*, No. CP4, Part 1, 1966, pp. 91–120.

[24] Townend, L. H., "On Lifting Bodies which Contain Two-Dimensional Supersonic Flows," Reports and Memoranda, No. 3383, 1964, Aeronautical Research Council, Great Britain.

[25] Cooke, J. C. and Jones, O. K., "The Boundary Layer on a Townend Surface," *Aeronautical Quarterly*, Vol. 16, No. 5, Part 2, April 1965, pp. 145–158.

[26] Cooke, J. C., "Supersonic Laminar Boundary Layers on Cones," TR 66347, 1966, Royal Aircraft Establishment.